

Pakistan Veterinary Journal

ISSN: 0253-8318 (PRINT), 2074-7764 (ONLINE) DOI: 10.29261/pakvetj/2025.296

RESEARCH ARTICLE

Functional Analysis of c-di-AMP Metabolic Proteins in a Bovine-Pathogenic *Bacillus cereus* Isolate

Zelin Jia ^{1#}, Qinglei Meng^{2#}, Haifeng Wang³, Ming Yu ³, Xin Zhang ¹, Jiayu Cui ¹, HuiSheng Xiong ¹, Yuhang Zhang ¹ and Xueli Wang ^{1*}

¹College of Animal Science and Technology, Inner Mongolia Minzu University, Tongliao 028000, China; ²College of Veterinary Medicine, Northeast Agricultural University, 600 Changjiang Road, Harbin 150030, China; ³Tongliao Institute of Agriculture and Animal Husbandry Sciences, Tongliao, 028015, China. [#] These authors contributed equally to this work. *Corresponding author: wangxl9577@aliyun.com

ARTICLE HISTORY (25-872)

Received: September 7, 2025 Revised: October 20, 2025 Accepted: October 23, 2025 Published online: November 17, 2025

Key words:

Cyclic diguanylate monophosphate Gene knockout Pathogenic bacillus cereus Virulence regulation

ABSTRACT

Bacillus cereus is a widespread Gram-positive pathogenic bacterium capable of producing toxins that induce severe illness or mortality in humans and animals. Cyclic diguanylate monophosphate (c-di-GMP), a bacterial second messenger, governs critical virulence traits such as biofilm formation and motility. While its regulatory role has been extensively characterized in Gram-negative bacteria, the functional significance of c-di-GMP in bovine pathogenic B. cereus remains poorly understood. Genomic analysis of the studied strain revealed a 5,484,345 bp chromosome and a 609,501 bp plasmid, harboring six c-di-GMP metabolism-associated genes (five encoding GGDEF domain-containing proteins and one encoding an EAL domaincontaining protein). Targeted gene knockout studies demonstrated that deletion of dgcl and eal significantly impaired biofilm formation, whereas disruption of dgc3 and dgc5 reduced motility. Notably, *dgc5* inactivation paradoxically enhanced biofilm development. No discernible phenotypic alterations were observed in dgc2 or dgc4 mutants. In murine infection models, eal-deficient strains accelerated host mortality. Histopathological examination confirmed organ damage induced by all mutant strains. This study provides the first systematic evidence highlighting the pivotal role of c-di-GMP metabolic genes in modulating virulence pathways of bovine pathogenic B. cereus, offering novel targets for therapeutic intervention.

To Cite This Article: Jia Z, Meng Q, Wang H, Yu M, Zhang X, Cui J, Xiong H, Zhang Y and Wang X, 2025. Functional analysis of c-di-AMP metabolic proteins in a bovine-pathogenic *bacillus cereus* isolate. Pak Vet J. http://dx.doi.org/10.29261/pakvetj/2025.296

INTRODUCTION

Bacillus cereus (B. cereus) is a Gram-positive bacterium exhibiting both probiotic properties and pathogenic potential. Certain strains can cause disease in animals and humans through toxin production(Saikia et al., 2024; Tong et al., 2024; Zhang et al., 2025). In recent years, cases of fatal infections in animals linked to B. cereus have been increasingly reported worldwide, highlighting the need for enhanced prevention, control, and safety assessment of its pathogenic variants(Chatelanat et al., 2024). Cyclic diguanylate monophosphate (c-di-GMP) is a ubiquitous bacterial second messenger that dynamically regulates key phenotypes including biofilm formation, motility, and virulence(Mao et al., 2025; Tawale, Ibrahim, and Aranjani, 2025). This signaling molecule is metabolized by proteins containing GGDEF (synthesizing) and EAL/HD-GYP (degrading) domains.

Although the regulatory mechanism of c-di-GMP in Gramnegative bacteria has been extensively (e.g., Pseudomonas aeruginosa, Vibrio parahaemolyticus and Escherichia coli), relatively few studies have focused on bovine-derived pathogenic B. cereus among Grampositive bacteria. (Chen et al., 2025a; Hermanas et al., 2021; Li et al., 2025; Ni et al., 2025; Wu et al., 2025). This study focuses on a highly pathogenic B. cereus strain isolated from the spleen of a cow that died suddenly. Using whole-genome sequencing and functional analyses, we systematically investigated the distribution and roles of cdi-GMP metabolic genes. By constructing gene deletion mutants and conducting phenotypic assays, we further explored the regulatory influence of the c-di-GMP signaling network on bacterial behaviors and virulence mechanisms. Our findings provide a theoretical foundation for controlling pathogenic B. cereus, support the development of novel antibacterial agents targeting c-diGMP pathways, and offer valuable insights for safety evaluation of probiotic strains.

MATERIALS AND METHODS

The bovine-derived pathogenic *B. cereus* strain Lycx, which exhibits high pathogenicity, was isolated from the spleen of suddenly deceased cattle by the Veterinary Pathology Laboratory at Inner Mongolia Minzu University. Competent cells of *Escherichia coli* strains DH5 α and HST04 were purchased from Takara Bio Inc.: DH5 α was used for cloning transformations, and HST04 was employed for methylation-deficient cloning. Six-week-old Kunming mice were obtained from Changchun Changsheng Biotechnology Co., Ltd.

following plasmids were used: pMD-The 19T (ampicillin resistance; used for cloning PCR products) ; pMAD (a temperature-sensitive shuttle vector for Grampositive bacteria. resistance carrying erythromycin/lincomycin and the β-galactosidase gene bgaB). SOC liquid medium (Cat. No.: CM1014L-01) was purchased from Shanghai Weidi Biotechnology Co., Ltd. Glycine (Cat. No.: G8200), sucrose (Cat. No.: S8271), and glycerol (Cat. No.: G8190) were purchased from Beijing Solarbio Science & Technology Co., Ltd. Hepes buffer (Cat. No.: ST2425) was purchased from Beyotime Biotechnology. MgCl₂ (Cat. No.: C0190529443) was purchased from Nanjing Reagent Co., Ltd. (used for the preparation of electrocompetent cells).

Genome sequencing and analysis of B. cereus: The Lycx strain was retrieved from storage at -80°C, resuscitated on Luria-Bertani (LB) agar, and cultured in LB broth. Bacterial cells were harvested and washed with sterile distilled water prior to genome sequencing, which was performed by BGI-Shenzhen using a combination of DNBSEQ and Nanopore platforms. Sequencing data were processed using the following tools: Glimmer (for gene prediction), Diamond (for homology alignment), and fastANI (for strain similarity analysis). Genomic components-including genes, non-coding RNAs, and CRISPR sequences-were identified, and functional annotation was carried out based on the COG, GO, and KEGG databases. Genes associated with c-di-GMP metabolism (those containing GGDEF, EAL, or HD-GYP domains) were specifically screened. Primer Premier 5 was used to design flanking primers for target genes; all oligonucleotides were synthesized by Sangon Biotech (Shanghai).

Construction of target Gene knockout vectors: Gene knockout vectors were constructed by targeting genes involved in c-di-GMP synthesis and degradation, which were initially identified through bioinformatics analysis of the whole genome sequence of the bovine-derived pathogenic *B. cereus* strain Lycx. Genomic DNA was extracted from the Lycx strain using a bacterial DNA extraction kit. Specific primers were designed to amplify the upstream and downstream homologous arms of each target gene by PCR, and the resulting fragments were verified by 1% agarose gel electrophoresis before being purified with a gel extraction kit. The purified PCR products were cloned into the pMD-19T vector and

transformed into *E. coli* DH5α competent cells. Positive clones were selected on ampicillin plates and further confirmed by colony PCR, double restriction enzyme digestion, and sequencing. Plasmids from validated clones were extracted, and the target fragments were recovered by double digestion and ligated into the similarly linearized pMAD shuttle vector, yielding the final knockout constructs (pMAD-*dgc1*, pMAD-*dgc2*, pMAD-*dgc3*, pMAD-*dgc4*, pMAD-*dgc5*, and pMAD-*eal*).

Genetic transformation and screening of positive clones: For genetic transformation and mutant screening. the knockout vectors were first introduced into E. coli DH5α via heat shock. Positive transformants were selected on ampicillin plates, and the correctness of the vectors was verified by restriction digestion, using the empty pMAD vector as a control. The confirmed plasmids were then transformed into the methylation-deficient E. coli HST04 strain using the same heat shock method, and positive clones were again validated by antibiotic selection, PCR, and enzyme digestion. In parallel, electrocompetent cells of the Lycx strain were prepared using the sucrose-glycine pretreatment method, with the specific steps as follows: Briefly, after the bacteria were revived and cultured, they were treated with sterile sucrose and glycine (treatment method: Glycine: 2.5 g, autoclaved at 121 °C for 20 min in solid state. Sucrose: 8.56 g, autoclaved at 121 °C for 20 min in solid state. Electroporation buffer: 250 mmol/L sucrose, 1 mmol/L Hepes, 1 mmol/L magnesium chloride, 10% glycerol, pH 7.0, sterilized at 121 °C for 20 min) (Wang, 2023). After further culture, the cells were pre-chilled on ice and then centrifuged. The cell pellet was collected, washed three times with ice-cold electroporation buffer, and finally resuspended and stored at -80 °C. For electroporation, 2 μL of the verified plasmid was mixed with the competent cells, and transformation was performed under the conditions of 1.8 kV voltage, 400 Ω resistance, and 4.9 ms pulse duration. After shaking recovery in SOC medium, the cells were plated on LB agar plates containing erythromycin (3 µg/mL), X-galactose (X-Gal, 20 μg/mL), and isopropyl-β-D-thiogalactoside (IPTG, 50 μg/mL), followed by incubation in the dark. Blue colonies were picked (blue colonies indicate single-crossover integrants) for subsequent processing.

Screening and validation of gene deletion mutants: Gene deletion mutants were obtained and verified through temperature induction and color-based screening. Blue colonies were picked and subjected to alternating cultivation at 30°C (permissive for replication) and 42°C promoting second homologous (restrictive, recombination) under erythromycin selection. White colonies appearing on X-Gal plates represented candidate mutants that had undergone double-crossover events and lost the knockout vector. These white colonies were cultured overnight at 30°C to obtain the final doublecrossover strains. Genomic DNA was extracted from the candidate mutants and analyzed by PCR using primers flanking the homologous regions. Successful gene deletion was confirmed by observing a size shift in the amplified fragments via agarose gel electrophoresis, followed by cloning and sequencing of the PCR products.

Phenotypic comparison of Gene deletion strains

Growth curves: Wild-type and mutant strains were inoculated into LB liquid medium. The optical density at 600 nm (OD₆₀₀) was measured every 2 hours over a 36-hour period (n=3).

Biofilm formation: Biofilms were cultured in tryptic soy broth (TSB) for 20 hours and quantified using crystal violet staining followed by measurement of OD₄₉₀ with a CCK-8 assay (n=3).

Enzyme activity and motility: Starch plates were used to assess hydrolysis zone formation, skim milk plates for protease activity, and semi-solid medium for motility diffusion diameter (n=3).

Mouse pathogenicity assay: The protocol was approved by the Ethics Committee of Inner Mongolia Minzu University (Approval No.: NMD-DW-2025-02-07). Sixweek-old specific pathogen-free (SPF) KM mice were acclimated for 7 days before grouping (n=6 per group). A total of 8 groups were set up, including the normal saline control group, wild-type strain Lycx group, Δdgc1 (dgc1 gene deletion) group, $\Delta dgc2$ (dgc2 gene deletion) group, $\Delta dgc3$ (dgc3 gene deletion) group, $\Delta dgc4$ (dgc4 gene deletion) group, $\Delta dgc5$ (dgc5 gene deletion) group, and Δeal (eal gene deletion) group. Mice in each group were intraperitoneally injected with 0.2 mL of sterile normal saline (negative control) or bacterial suspension of wildtype strain/gene deletion mutants (OD₆₀₀= 0.5 ± 0.05). The bacterial concentration was adjusted to 10° CFU/mL using the McFarland turbidity method. Clinical indicators were observed daily. Mice that reached the humane endpoint were euthanized by CO₂ anesthesia; those surviving until 72 h were euthanized by cervical dislocation after isoflurane anesthesia. Organs were fixed in 10% neutral buffered formalin, embedded in paraffin, sectioned at 4 µm, stained with hematoxylin and eosin (HE), and subjected to histological evaluation in a double-blind manner.

RESULTS

Whole-Genome Sequencing of *B. cereus* Genomic Overview and Identification of c-di-GMP-Related Genes: The genome of *B. cereus* strain Lycx comprises a single chromosome of 5,484,345 bp (GC content 35.39%) and one plasmid of 609,501 bp (GC content 32.16%). The complete genome sequence has been deposited in the NCBI GenBank database under accession numbers CP129005 (chromosome) and CP129006 (plasmid). A total of 6,011 protein-coding genes were predicted, along with various non-coding RNAs (including tRNAs, rRNAs, and sRNAs; see Table 1) and several CRISPR arrays (Fig. 1A, 1B; Table 2).

Functional annotation and Genomic features of the sequenced strain: Functional annotation identified 325 virulence factor genes and 59 antimicrobial resistance genes in the *B. cereus* Lycx strain, which are implicated in 44 KEGG pathways. Additionally, six genes involved in c-di-GMP metabolism were identified. Among these, *dgc1* and *dgc4* contain a GGDEF domain, *dgc2*, *dgc3*, and *dgc5* contain tandem GGDEF–EAL domains, and *eal* contains an EAL domain. A summary of 11 key genes

is provided in Table 3. COG annotation classified 4,145 genes into four major functional categories (Fig. 1C): Cellular processes and signaling (27.6%, including cell cycle control and signal transduction); Information storage and processing (18.7%, covering replication, recombination, and translation); Metabolism (39.9%, including amino acid and carbohydrate metabolism); Poorly characterized or unknown function (13.8%).

Table 1: Statistical results for non-coding RNA

Type of Non-	Сору	Average	Total Length of	Percentage of
coding RNA	Number	Length	Non-coding RNA	Non-coding RNA
				in the Genome
tRNA	107	77 bp	8251 bp	0.1354 %
5S-rRNA	14	115 bp	1610 bp	0.0264 %
16S-rRNA	14	1539 bp	21551 bp	0.3536 %
23S-rRNA	14	2919 bp	40868 bp	0.6706 %
sRNA	48	97 bp .	4676 bp	0.0767 %

Table 2: Statistical results of CRISPR

CRISPR ID	Predicted	Predicted	Predicted
	Starting Position	Ending Position	Regional Length
	of CRISPR	of CRISPR	of CRISPR
Chromosome I-I	2 437 622 bp	2 437 719 bp	97 bp
Chromosome I-2	2 973 317 bp	2 973 473 bp	156 bp
Chromosome I-3	3 358 904 bp	3 359 714 bp	810 bp
Chromosome I-4	3 360 002 bp	3 360 082 bp	80 bp
Chromosome I-5	5 267 312 bp	5 267 445 bp	133 bp

Table 3: Annotation results statistics for gene sets

Name	B. cereus. lycx	
Total number of genes	6011	
VFDB	325	
ARDB	59	
CAZy	236	
Swiss-Prot	2777	
COG	4145	
CARD	7	
GO	3196	
KEGG	3265	
NR	5976	
T3SS	698	

GO annotation assigned 3,192 genes to three functional categories (Fig. 1D): Cellular component (11.8%, e.g., cellular anatomical entities); Molecular function (37.4%, such as catalytic activity and protein binding); Biological process (50.8%, including metabolic and regulatory processes).

KEGG pathway analysis revealed involvement in 44 pathways, grouped into six major categories (Fig. 1E). The majority of genes (2,384) were associated with metabolic pathways, encompassing 12 subcategories such as carbohydrate metabolism, amino acid metabolism, and metabolism of cofactors and vitamins. Other notable categories included environmental information processing (406 genes) and genetic information processing (231 genes).

Comparative Genomic analysis: The genome of the sequenced *B. cereus* Lycx strain was compared with those of five reference strains (Table 4), including: *B. cereus* 3AES (a U.S. Food and Drug Administration (FDA) standard strain used for rapid detection of foodborne outbreaks; GenBank accession: CFSAN109650); *B. cereus* SCBCM (isolated from *Moschus berezovskii* in Sichuan, China; accession: ASM2959037v1); *B. cereus* ACH28 (isolated from dairy farm equipment and cows in Australia; accession: ASM1507111v1); *B. cereus* C3514 (isolated from camel feces in Hong Kong, China; accession: ASM327003v1); *B. cereus* E33L

(isolated from a dead zebra carcass in Namibia; accession: ASM1162v1).

Average nucleotide identity (ANI) analysis revealed that the test strain (*B. cereus* Lycx) shared the highest identity (97.85%) with *B. cereus* SCBCM (from *Moschus berezovskii*), followed by the FDA reference strain 3AES (97.09%), *B. cereus* C3514 (91.62%), *B. cereus* E33L (91.30%), and *B. cereus* ACH28 (88.62%) (Fig. 1F). A phylogenetic tree constructed based on gene family analysis further supported the closest evolutionary relationship between the test strain and *B. cereus* SCBCM

(Fig. 2A). Comparative analysis of gene families among all six strains is summarized in Fig. 2B.

Table 4: Strain gene information sheet

Name	Number of Genes Number of genes Number of Genes		
	in the Strain	containing N's	Used for Analysis
B. cereus. lycx	6011	0	6011
B. cereus. SCBCM	15 587	3	5 584
B. cereus. E33L	5 661	3	5 658
B. cereus. C3514	5 204	206	4 998
B. cereus. ACH28	5 609	39	5 570
B. cereus. 3AES	5 154	22	5 132

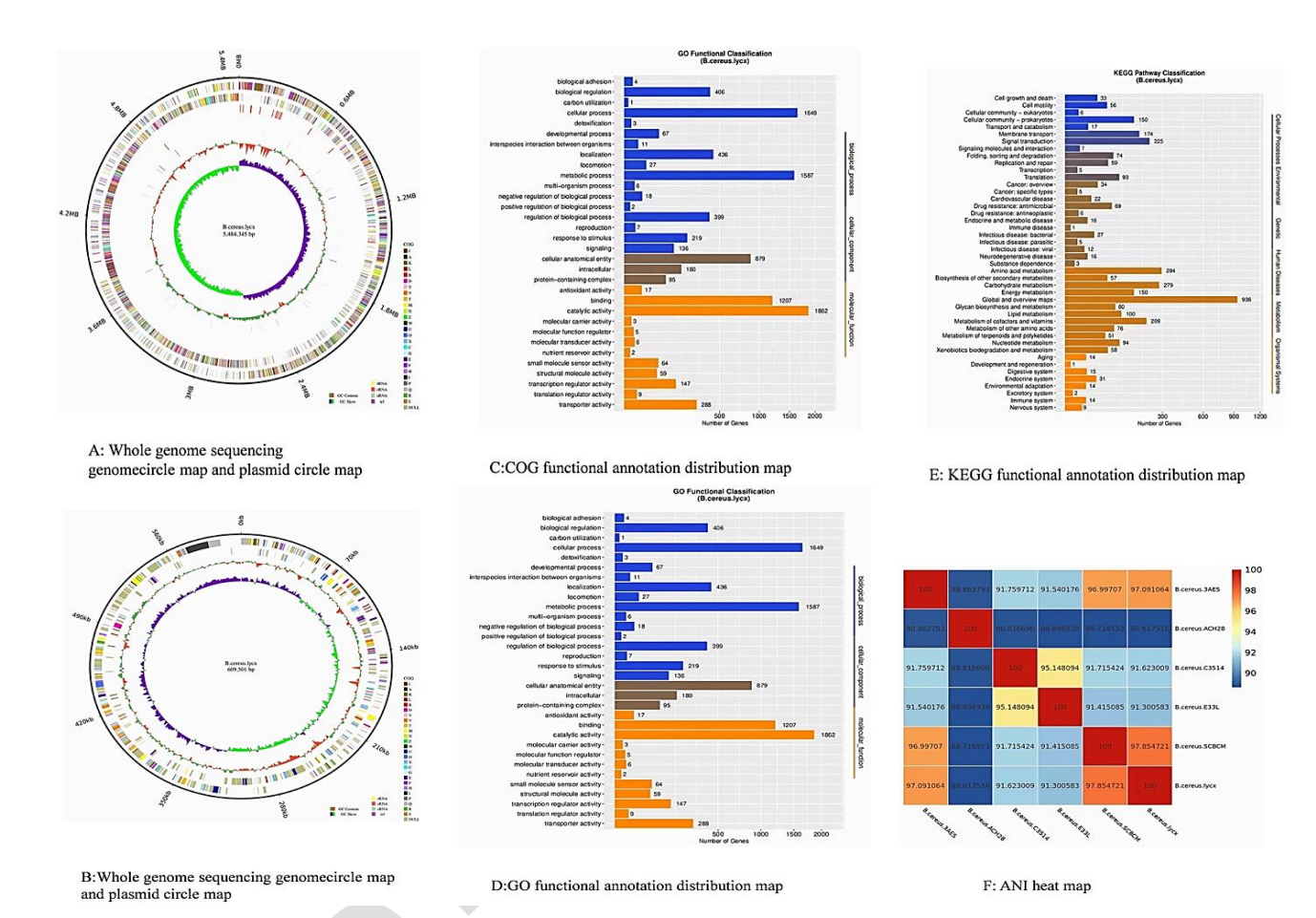


Fig. I: Genome and Functional Annotation Analysis of Strains.

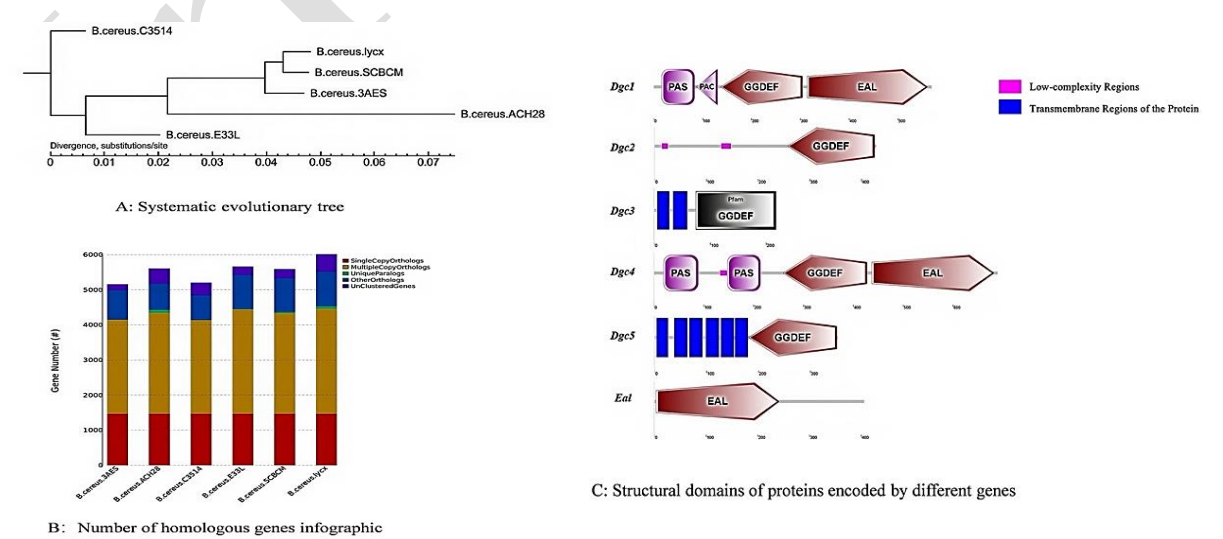


Fig. 2: Phylogenetic and Gene-Protein Structural Analysis of Bacillus cereus.

Identification and analysis of c-di-GMP metabolism-**Related Genes:** Bioinformatic analysis identified six genes in the test strain implicated in c-di-GMP metabolism (Fig. 2C). The encoded proteins were categorized as follows: Proteins containing a GGDEF domain: Dgc1 (1,710 bp, 569 amino acids) and Dgc2 (1,293 bp, 430 aa); Proteins containing tandem GGDEF-EAL domains: Dgc3 (654 bp, 217 aa), Dgc4 (2,070 bp, 689 aa), and Dgc5 (1,059 bp, 352 aa); A protein containing an EAL domain: Eal (1,218 bp, 405 aa). Based on their domain architectures, these proteins are predicted to be involved in c-di-GMP synthesis (via the GGDEF domain) and degradation (via the EAL domain), respectively.

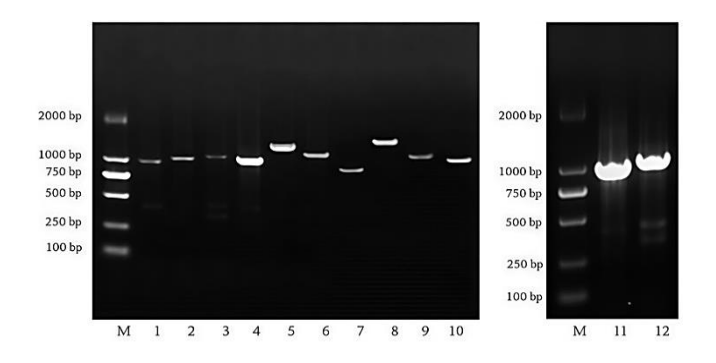
Construction of Gene deletion mutants

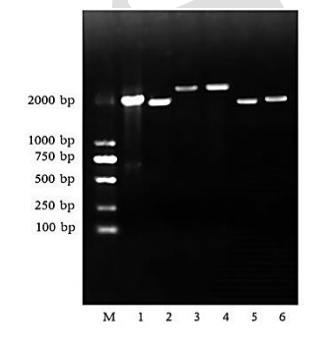
Amplification and cloning of flanking regions: The upstream and downstream regions of each target gene were amplified from genomic DNA of the test strain using genespecific primers (Fig. 3A). The purified PCR products were ligated into the pMD19-T vector and transformed into E. coli DH5α competent cells. Positive clones were selected on ampicillin (100 µg/mL) and verified by PCR, double

restriction digestion, and sequencing (Fig. 3B). The linearized plasmid was subsequently purified for use in vector construction.

Assembly of knockout vectors and transformation: The fused upstream-downstream fragments were ligated into the dual-digested and linearized pMAD vector to generate the knockout constructs (Fig. 4A). Each recombinant vector was transformed into E. coli HST04 competent cells. Positive transformants were selected using ampicillin and confirmed by PCR and restriction digestion.

Generation and verification of deletion mutants: The knockout vectors were introduced into B. cereus competent cells via electroporation. Blue colonies (indicating singlecrossover events) were selected on plates containing erythromycin (3 μg/mL) and X-Gal. Following induction of a second crossover at 42 °C, white colonies (doublecrossover mutants) were isolated on X-Gal plates. PCR analysis confirmed a smaller amplicon in the mutants compared to the wild-type strain (Fig. 4B), and sequencing results verified the successful deletion of each target gene.





A: PCR results of the upper and lower fragments of the target

Note: M, DL2000 DNAMarker; 1, Dgc1-u; 2, Dgc1-d; 3, Dgc2-u; 4, Dgc2-d; 5, Dgc3-u; 6, Dgc3-d; 7, Dgc4-u; 8, Dgc4-d; 9, Dgc5-u; 10, Dgc5-d; 11, Eal-u; 12, Eal-d.

B: Plot of PCR results of ligated fragments

- Note: M, DL2000 DNAMarker;

 1, Upstream and downstream linkage fragments of the *Dgc1* gene;

 2, Upstream and downstream linkage fragments of the *Dgc2* gene;

 3, Upstream and downstream linkage fragments of the *Dgc3* gene;

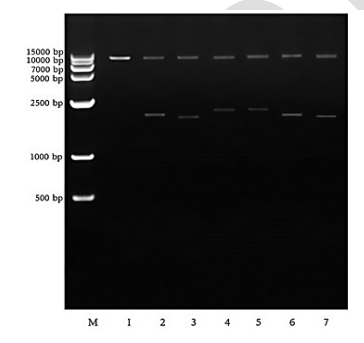
 4, Upstream and downstream linkage fragments of the *Dgc4* gene;

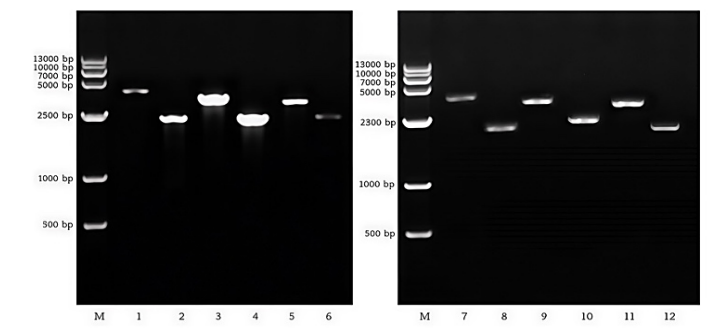
 5, Upstream and downstream linkage fragments of the *Dgc5* gene;

 6, Upstream and downstream linkage fragments of the *Dgc5* gene;

- 6. Upstream and downstream linkage fragments of the Eal gene

Fig. 3: Electrophoretogram of PCR Amplification and Ligation Fragment Verification of Target Genes.





A: Plot of zymographic validation results of knockout vectors

ote: M, DL15000 DNAMarker;

Note: M, DLI JOUD D'NAMARK, 1, PMAD empty vector digest; 2, PMAD-Dgc; 3, PMAD-Dgc2; 4, PMAD-Dgc3; 5, PMAD-Dgc4; 6, PMAD-Dgc5; 7, PMAD-Eal.

B: Graph of validation results of knockout genes

D. CHAPIT OF VARIGATION FESTIRES OF KNOCKOUT GETES

Note: M, DL 15000 DNAMArker; 1,2 indicates the results of amplifying normal strain DNA and Dgc1 gene deletion strain DNA with upstream and downstream primers of Dgc1 gene; 3,4 indicates the results of amplifying normal strain DNA and Dgc2 gene deletion strain DNA with upstream and downstream primers of Dgc2 gene; 5,6 indicates the results of amplifying normal strain DNA and Dgc3 gene deletion strain DNA with upstream and downstream primers of Dgc3 gene; 7,8 indicates the results of amplifying normal strain DNA and Dgc4 gene deletion strain DNA with upstream and downstream primers of Dgc4 gene The results of upstream and downstream primers of Dgc3 gene were used to amplify DNA of normal strain and DNA of Dgc3-deficient strain; 7,8 indicated the results of upstream and downstream primers of Dgc4 gene were used to amplify DNA of normal strain and the results of upstream and downstream primers of Dgc4 gene were used to amplify DNA of normal strain and DNA of Dgc4-deficient strain; 9,10 indicated the results of upstream and downstream primers of Dgc5 gene were used to amplify DNA of normal strain and DNA of Dgc5-deficient strain; 1,12 indicated the results of upstream and downstream primers of Ed 11,12 are the results of amplifying DNA of normal strain and DNA of EdI-deficient strain with upstream and downstream primers of Eal gen

Fig. 4: Electrophoretogram of Enzymatic Validation of Knockout Vectors and PCR Validation of Knockout Strains.

Phenotypic characterization of wild-Type and Gene deletion mutants

Growth curves: Growth curves were generated for the wild-type *B. cereus* and each mutant strain cultured on LB liquid medium (Fig. 5A). The growth of *dgc3* and *dgc5* mutants was comparable to that of the wild-type strain during the lag and logarithmic phases. However, upon entering the stationary phase, both mutants exhibited slightly enhanced growth relative to the wild type. The remaining mutants showed no significant differences in growth compared to the wild-type strain.

Results of biofilm metabolism determination: Biofilm formation was assessed using crystal violet staining. The *dgc5* mutant exhibited increased biofilm production, while the *dgc1* and *eal* mutants showed reduced biofilm formation. No significant changes were observed in the other mutants (Fig. 5B). Metabolic activity within the biofilms was further evaluated using a CCK-8 assay, with data analyzed using

GraphPad Prism software. Results confirmed that deletion of dgc5 enhanced biofilm formation, whereas deletion of dgc1 or eal impaired it (Fig. 5C). The other gene deletions had no notable impact on biofilm-forming capability.

Extracellular amylase activity: Amylase production was evaluated on starch plates. All six mutant strains and the wild type formed clear hydrolysis zones around the colonies, indicating retained amylase activity (Fig. 6A). The hydrolysis capacity—calculated as the ratio of the zone diameter to the colony diameter—was similar between mutants and the wild type (wild type: 1.45 ± 0.03). These results suggest that deletion of the six target genes did not significantly affect extracellular amylase production.

Extracellular protease activity: Protease activity was assessed on skim milk plates. All strains produced transparent hydrolysis zones, confirming extracellular protease production (Fig. 6B). The hydrolysis capacity

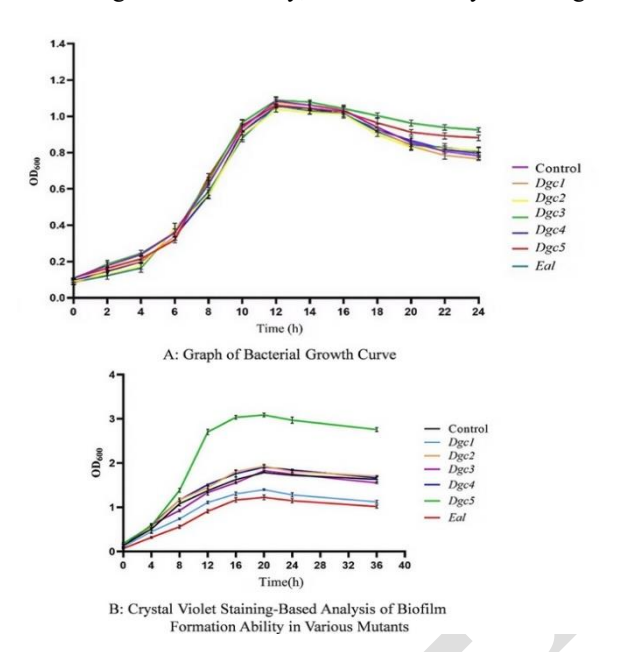
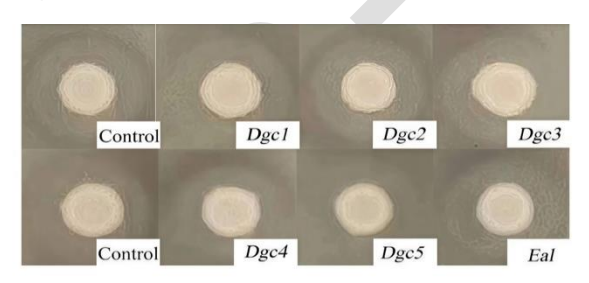
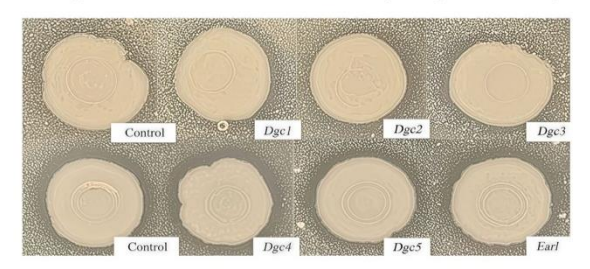


Fig. 5: Analysis of Strain Growth and Biofilm Characteristics

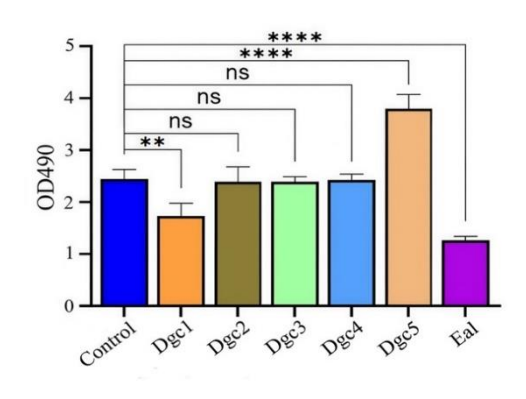


A: Comparison of bacterial extracellular amylase production capacity

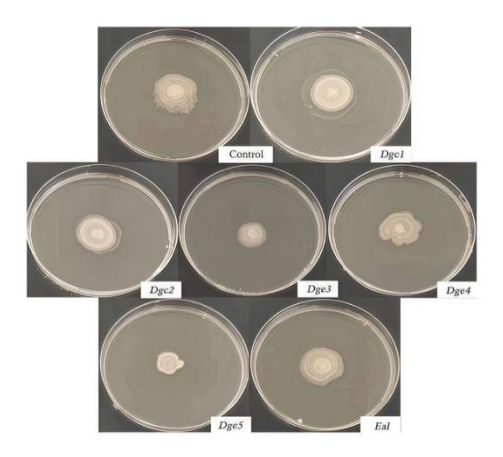


B: Comparison of bacterial extracellular protease production capacity

Fig. 6: Analysis of Extracellular Enzyme Secretion and Motility of Strains.



C: Comparison Chart of Biofilm Metabolic Activities in Different Strains Determined by CCK-8



C: Comparison of motility of different strains of bacteria

values were comparable between mutants and the wild type (wild type: 1.15 ± 0.02), indicating that gene deletion did not alter protease production.

Bacterial motility: Motility assays were conducted in semi-solid medium over 48 hours (Fig. 6C). The dgc3 (1.72 \pm 0.025 cm) and dgc5 (1.88 \pm 0.032 cm) mutants exhibited significantly reduced motility compared to the wild type (2.82 \pm 0.017 cm). Motility of the other mutants was not significantly affected, indicating that dgc3 and dgc5 play specific roles in bacterial movement.

Histopathological analysis in mice: Most mice in the control group (injected with wild-type strain Lycx group) and the Δeal mutant group died within 3-6 hours postinjection. In the remaining mutant groups, some mice died around 6 hours, and all succumbed within 8 hours. The death timeline is shown in Table 5, and the results of pathological sections are presented in Fig. 7. In the pathological tissue sections of the wild-type strain Lycx group: Cardiomyocytes showed granular degeneration, with cell swelling and fragmentation; some areas exhibited waxy necrosis, and a small amount of inflammatory cell infiltration was observed between myocardial fibers. The central veins of the liver were significantly dilated; hepatocyte nuclei near the central veins were fragmented, dissolved, and disappeared. Sinusoids were dilated, with a small amount of red blood cell infiltration. The splenic pulp was filled with a large amount of blood, and splenic parenchymal cells showed local disintegration and necrosis. Capillaries in the alveolar walls were significantly dilated; a large number of red blood cells and white blood cells filled the lumens of some alveoli. Renal tubular epithelial cells underwent degeneration, necrosis, and shedding, and local glomeruli showed atrophy. In the Dgc1 group, Myocardial fibers showed granular degeneration, with scattered red blood cell infiltration between them. The central veins of hepatic lobules and the surrounding sinusoids were dilated, filled with red blood cells; hepatocytes around the lobules exhibited granular degeneration. A small number of lymphocytes and reticular cells in the spleen underwent necrosis, with their nuclei dissolved or fragmented, and cytoplasm swollen and disintegrated; a few cells still had pale-staining and swollen nuclei. Capillaries in the alveolar walls were congested; varying amounts of red blood cells and a small number of neutrophils were present in individual alveoli. Glomerular capillaries were congested; renal tubular epithelial cells underwent necrosis and shedding, and individual glomeruli showed necrosis. In the Dgc2 group, Myocardial fibers were fragmented, with a large amount of red blood cell infiltration between them. Hepatocyte nuclei near the central veins of the liver disappeared, and hepatocytes underwent necrosis, leaving only pale-staining cell outlines. A small number of lymphocyte nuclei in the spleen disappeared, and scattered necrotic foci were observed in the white pulp. Capillaries in the alveolar walls were significantly congested; a large number of red blood cells and white blood cells filled the lumens of individual alveoli. Epithelial cells of *Bowman's capsules* proliferated; individual renal tubular epithelial cells underwent shedding and necrosis. In the Dgc3 group, Myocardial fibers were

swollen, with a small amount of red blood cell infiltration between them. Hepatic sinusoids near the central veins were significantly dilated, with a small number of red blood cells; most hepatocytes exhibited granular degeneration. In multiple areas of the splenic red pulp, lymphocytes and reticular cells underwent necrosis, with their nuclei disappeared and only cell outlines remaining. Capillaries in the alveolar walls were significantly congested; a large number of red blood cells and white blood cells filled the lumens of individual alveoli. Glomerular capillaries were congested; mesangial cells proliferated, and epithelial cells of Bowman's capsules proliferated. In the Dgc4 group, Myocardial fibers were swollen and fragmented, with a small amount of inflammatory red blood cell infiltration between them. The central veins and sinusoids of the liver were significantly dilated, with a small number of red blood cells in the sinusoids; most hepatocyte nuclei in the peripheral regions of hepatic lobules disappeared, and hepatocytes underwent necrosis. Most lymphocytes in the spleen underwent severe necrosis, with pale-staining nuclei. Capillaries in the alveolar walls were significantly dilated and congested; some alveoli showed collapse. Glomerular mesangial cells proliferated; some renal tubular epithelial cells underwent shedding and necrosis. In the Dgc5 group, Myocardial fibers were swollen and fragmented, with a large amount of inflammatory red blood cell infiltration between them. The central veins of the liver were dilated; a small number of red blood cells were present in the sinusoids; most hepatocyte nuclei were fragmented, dissolved, and disappeared. Most lymphocytes in the splenic germinal centers underwent necrosis, with cell dissolution and disappearance. Capillaries in the alveolar walls were significantly dilated and congested; the lumens of individual alveoli were filled with red blood cells and white blood cells. Glomerular capillaries were congested; renal tubular epithelial cells shed and disappeared, and renal tubules underwent necrosis. In the Eal group, Myocardial fibers were swollen fragmented, with a small amount of red blood cell infiltration between them. The central veins of the liver were significantly dilated; hepatocyte nuclei near the central veins disappeared, and hepatocytes underwent necrosis. Scattered necrotic foci were observed in both the white pulp and red pulp of the spleen; among these, a small number of lymphocytes and reticular cells had undergone necrosis, with their nuclei dissolved or fragmented. Capillaries in the alveolar walls were dilated; a large number of red blood cells and white blood cells filled the lumens of individual alveoli. Glomerular capillaries were congested; exuded white blood cells and red blood cells were present in the Bowman's capsules lumens. Renal tubular epithelial cells underwent degeneration and necrosis.

Table 5: Mouse Mortality Table

Table 3. House Hortality	i abie.
Group	I - 3h 3 - 4h 4 - 5h 5 - 6h 6 - 7h 7 - 8h
Control group	0 dead 0 dead 0 dead 0 dead 0 dead
Wild-type strain Lycx	0 dead 2 dead 1 dead 1 dead 2 dead 0 dead
group	
Dgc1 gene deletion group	0 dead 0 dead 0 dead 1 dead 3 dead
Dgc2 gene deletion group	0 dead 0 dead 1 dead 0 dead 3 dead 2 dead
Dgc3 gene deletion group	0 dead 0 dead 1 dead 2 dead 3 dead
Dgc4 gene deletion group	0 dead 0 dead 1 dead 1 dead 3 dead 1 dead
Dgc5 gene deletion group	0 dead 0 dead 0 dead 2 dead 2 dead 2 dead
Eal gene deletion group	0 dead 2 dead 1 dead 3 dead 0 dead 0 dead

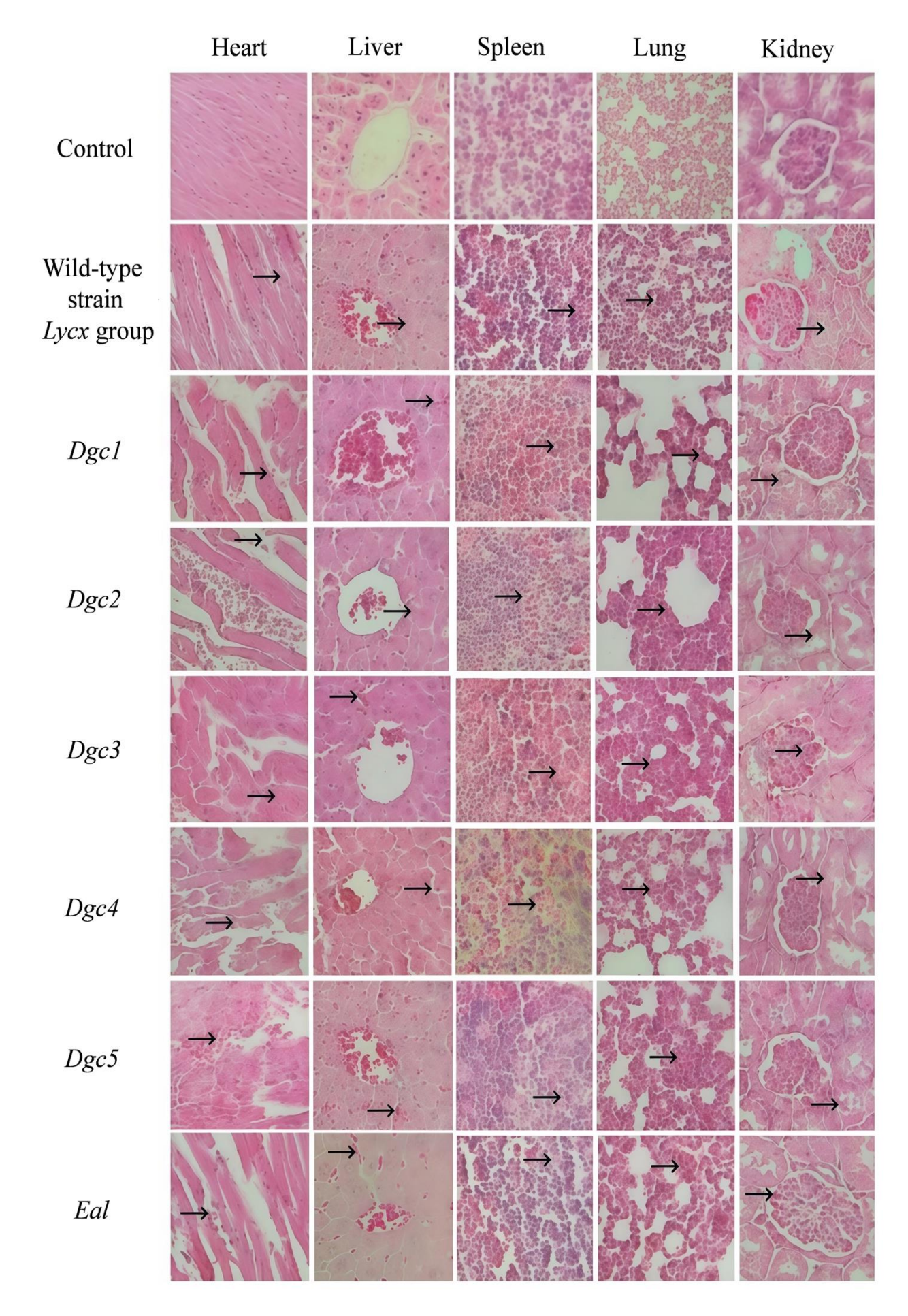


Fig.7: Pathological sections of mice with different strains (400 \times).

DISCUSSION

a peritrichously flagellated, Gram-B. cereus, positive bacterium, exerts its pathogenicity primarily through the production of diverse toxins that disrupt host immune defenses, cause food poisoning, and induce tissue damage. The hemolysin BL (HBL) and non-hemolytic enterotoxin (NHE) act synergistically to provoke inflammation(Fox et al., 2020; Ramm et al., 2021), while the emetic toxin cereulide not only triggers acute gastrointestinal symptoms but can also lead to acute hepatic failure(Mahler et al., 1997; Schreiber et al., 2021). Successful colonization of the gastrointestinal tract essential for causing diarrhea or food poisoning—requires the bacterium to adapt to both the acidic environment (pH 1.5-5) and shifting oxygen concentrations, from aerobic to anaerobic conditions(Duport, Jobin, and Schmitt, 2016). In the pathological sections from our experimental infection model, evident lesions such as granular degeneration of cardiomyocytes, hepatic necrosis, and renal tubular epithelial cell desquamation were observed. These pathological changes are closely associated with the direct effects of bacterial toxins and the inflammatory responses they elicit. Collectively, our findings underscore the critical role of toxin-mediated damage and inflammation in B. cereus pathogenesis.

The spores are capable of germinating under favorable circumstances, leading to food spoilage and potential health risks for humans and animals(Heydenreich et al., 2025; Mustafa et al., 2025). Biofilms formed by B. cereus on solid surfaces, within liquids, or at air-liquid interfaces can also adversely affect food processing equipment. Additionally, some strains possess a surface layer (S-layer) structure that facilitates host cell invasion and confers resistance to external stressors (Komprda et al., 2025; Mustafa, Abo-Kamer, and Al-Madboly, 2025; Subanna et al., 2025; Sun et al., 2025). In recent years, cases of sudden animal death due to pathogenic B. cereus have been reported across China, affecting species such as the Chinese soft-shelled turtle (Pelodiscus sinensis), cattle, and pigs(Calvigioni et al., 2022; Fang et al., 2025; Fei et al., 2019; Xiao et al., 2023). The ability of B. cereus to form spores and biofilms com disease prevention and control. Although large-scale outbreaks have not yet been recorded, the high virulence of pathogenic strains and the resilience of their spores pose significant challenges for eradication(Baek et al., 2025; Leguérinel et al., 2025).

The second messenger cyclic di-GMP (c-di-GMP) is widely distributed among microorganisms and regulates multiple physiological processes, such as biofilm formation, motility, and extracellular enzyme production. The number of proteins containing GGDEF and EAL domains varies considerably across bacterial species, and some of these proteins exhibit non-conserved domain architectures. While c-di-GMP signaling has been extensively studied in Gram-negative bacteriaincluding Escherichia coli, Pseudomonas fluorescens, Pseudomonas aeruginosa, Burkholderia cenocepacia, and Salmonella—where elevated c-di-GMP levels promote biofilm formation, inhibit motility, and modulate virulence(Chen et al., 2025b; Fazli et al., 2014; Povolotsky and Hengge, 2012; Römling, Galperin, and Gomelsky,

2013; Toyofuku et al., 2016), research in Gram-positive bacteria remains relatively limited. In Bacillus subtilis, for example, c-di-GMP regulates swarming motility but does not influence biofilm formation(Gao et al., 2013; Kunz et al., 2020). The B. cereus group comprises several clinically and economically important species, such cereus (associated with sudden cattle death as in this study), Bacillus anthracis, and Bacillus thuringiensis, in which biofilm formation is closely linked to environmental adaptation and virulence. Genomic analysis of this group Annette Fagerlund et al. (Fagerlund 2016)identified 13 putative cdg genes encoding proteins with GGDEF, EAL, or HD-GYP domains, among which 10 core genes (cdgA-J) were conserved in over 85% of the strains, including B. anthracis. Using B. thuringiensis 407 as a model, the authors demonstrated that cdgF acts as a master regulator of aerobic biofilm formation: its deletion abolished biofilms, while its overexpression enhanced biofilm formation sixfold. CdgF functions as a bifunctional enzyme, primarily displaying diguanylate cyclase (DGC) activity under oxidizing conditions to synthesize c-di-GMP, while increasing phosphodiesterase (PDE) activity under reducing conditions to degrade it. Elevated c-di-GMP levels promoted biofilm formation, inhibited motility, and reduced cytotoxicity, as evidenced by decreased secretion of NheB and CytK toxins. Furthermore, cdgE (a PDE-encoding gene) inhibited biofilm, and cdgC (enzymatically inactive) regulated sporulation. Notably, the c-di-GMP signaling network in the B. cereus group shares only two homologous genes with that of B. subtilis, underscoring its unique role in regulating the lifestyle of this group. Whitfield et al.(Whitfield et al., 2020) proposed that biofilm formation in B. cereus is co-regulated by the synthase CdgF and the degrading enzyme CdgE, which aligns with the roles of Dcg1 and Dcg2 identified in the present study.

The bacterial strain used in this study was isolated from the spleen of a cow that died suddenly in our laboratory. Previous findings have demonstrated that this strain exhibits strong survival capacity under adverse conditions, together with robust biofilm-forming ability and pathogenicity. In the present work, we performed whole-genome sequencing of the strain followed by comprehensive bioinformatic analysis. Based annotations from the Virulence Factor Database (VFDB) and the Comprehensive Antibiotic Resistance Database (CARD), a total of 325 virulence genes and 59 antibiotic resistance-related genes were predicted in its genome. It should be noted that from 2018 to 2025, our team had already investigated a subset of these virulence genes in prior studies(Chen et al., 2023; Meng et al., 2025; Song, 2019). Moreover, the antibiotic resistance genes identified via CARD—which include antibiotic target genes—only indicate the potential genetic determinants of resistance and do not necessarily confer phenotypic resistance to all corresponding antibiotics. In earlier published work, we conducted antimicrobial susceptibility testing using clinically relevant antibiotics and found the strain to be susceptible to cefalexin, cefazolin, gentamicin, and norfloxacin; intermediately susceptible to cefoperazone, tetracycline, and polymyxin B; and resistant to penicillin, neomycin, and clindamycin. These results further underscore that genomic prediction of resistance genes

does not always translate into broad phenotypic resistance, highlighting the necessity of experimental validation to accurately determine the resistance profile.

Prior to obtaining the genomic data, primer design depended on reference strains and published sequences. However, as reference strains are often probiotic and genetically distinct from pathogenic isolates, this approach risked poor primer specificity and amplification failure due to sequence divergence or absence of target genes. The genomic sequence obtained here provides a reliable basis for strain-specific investigations.

In this study, we identified and knocked out genes involved in c-di-GMP synthesis and degradation using molecular techniques. We then compared phenotypic traits—including motility, biofilm formation, and growth—between the wild-type and mutant strains. Deletion of specific genes resulted in distinct phenotypic changes: dgc1 showed reduced biofilm formation without other changes; dgc2 exhibited no significant differences from the wild type; dgc3 displayed enhanced stationary-phase growth and reduced motility; dgc4 was similar to the wild type; dgc5 showed improved stationary-phase growth, reduced motility, and enhanced biofilm formation; eal had reduced biofilm formation. Notably, biofilm formation and motility were not inversely correlated; reduced biofilm did not necessarily coincide with increased motility.

The construction of pathological section models aims to bridge the "in vitro gene function" with "in vivo pathogenic effects." Acute mortality in mice (within hours) after injection of different bacterial suspensions may be caused by potent toxins secreted by bacteria or excessive inflammatory responses and septic shock triggered by large amounts of bacterial components, rather than relying on the massive proliferation of bacteria in vivo. This is consistent with the known characteristic of B. cereus to produce various virulence factors such as enterotoxins and hemolysins. Observation of pathological changes in the core organs of mice via HE staining directly confirms the invasive ability of bovine-derived pathogenic B. cereus against the host. Obvious changes in pathological tissue sections show typical lesions in mice of the wild-type strain group, including granular degeneration cardiomyocytes, hepatocyte necrosis, and disintegration of splenic parenchymal cells. These changes intuitively verify that the strain can break through the host's immune barrier and induce multi-organ damage, providing in vivo experimental evidence for "the strain having strong pathogenicity." Particularly crucially, although deletion of the eal gene impairs biofilm formation in vitro, it significantly enhances bacterial virulence in vivo, leading to shortened death time of mice and more severe organ lesions. This strongly suggests that the degradation process of c-di-GMP is crucial for inhibiting acute virulence factors. Meanwhile, the enhanced biofilm formation and reduced motility in vitro caused by dgc5 deletion are also translated into more significant pathological damage to the spleen and lungs in vivo, completing the regulatory chain from "gene" to "phenotype" and then to "pathogenicity."

In the realm of medicine and public health, infections associated with bacterial biofilms represent a growing and serious challenge. The drug resistance exhibited by bacterial biofilms arises from their complex architecture and unique microenvironment, which operate through two

primary mechanisms. On one hand, bacteria produce extracellular polymeric substances (EPS) that form a dense physical barrier—composed of polysaccharides, proteins, extracellular DNA, and other components—that effectively blocks host immune clearance and impedes antibiotic penetration. On the other hand, the distinctive microenvironment within biofilms, such as hypoxia and acidic conditions, alters bacterial physiology and further compromises antibiotic efficacy, thereby establishing a dual resistance strategy combining "physical barrier and adaptive microenvironment." Treating biofilm-related requires achieving multiple infections simultaneously: disrupting the EPS barrier to release embedded bacteria into a planktonic state, dismantling the overall biofilm structure to prevent re-aggregation, and thoroughly eradicating both freed and residual pathogenic bacteria. Failure to meet these goals may lead to disseminated infection, as bacteria released from biofilms often exhibit enhanced virulence, potentially worsening disease progression and triggering severe toxic side effects.

Based on the current research status, breakthrough paths can be explored from multiple dimensions in the future. innovative strategies can be explored across multiple dimensions. At the molecular level, gene interference technologies may inhibit biofilm formation, and novel agents could be developed to target key functional genes-such as gene-targeted drugs directed against B. cereus biofilms. In terms of behavioral control, regulating bacterial motility may reduce transmission and disease outbreaks, while also providing insights into diversity. Additionally, bacterial community regulatory mechanisms and enzymatic activities influencing pathogenicity and viability may offer new intervention targets, paving the way for integrated therapeutic strategies centered on "disruption-clearanceprevention".

In pathogenic B. cereus various genes regulate distinct biological traits. Certain proteins harbor tandem GGDEF-EAL domain architectures, such as those encoded by dgc2, dgc3, and dgc5. Although bioinformatic analyses suggest these genes may possess diguanylate cyclase (DGC) activity, sequence alignment of their domains with core cdg genes from the B. cereus group-such as cdgF from Bacillus thuringiensis 407—reveals amino acid substitutions at key catalytic sites within the GGDEF domains. These alterations may lead to reduced DGC activity or functional divergence, potentially explaining why deletion of dgc2 and dgc4 does not significantly alter bacterial phenotypes. Similarly, deletion of the eal gene reduces biofilm formation without markedly affecting other traits, possibly due to the relative functional plasticity of the EAL domain, which may operate through redundant pathways or in concert with other phosphodiesterases (PDEs). Given the complexity of c-di-GMP-mediated regulation in bacteria, single-gene deletions often yield only subtle phenotypic changes. A key limitation of this study is the absence of complementation strains to fully confirm genotype-phenotype relationships. Future work should prioritize functional validation via genetic complementation to clarify the precise regulatory network of c-di-GMP in bovine-derived pathogenic B. cereus. Overall, this study provides preliminary evidence that

modulating c-di-GMP levels influences several biological traits in this pathogen, offering insights for mechanistic studies and suggesting new avenues for molecular drug development and disease control strategies targeting *B. cereus*.

Declarations:

Ethics approval and consent to participate: All animal experiments were approved by the Medical and Life Science Ethics Committee of Inner Mongolia Minzu University (Protocol No NMD-DW-2025-02-07) and adhered to ARRIVE guidelines. Agree to participate and publish.

Consent for publication: Not applicable. This study did not involve human participants.

Funding: This work was supported by the Multidisciplinary Interdisciplinary Research Project of Basic Scientific Research Operating Expenses for Colleges and Universities directly under Inner Mongolia under Grant GXKY22003.

Availability of data and materials: All data generated or analyzed during this study are included in this published article. No additional datasets were deposited in external repositories.

Acknowledgements: I would like to thank Prof. Xue-Li Wang and my labmates for their help, and I am very grateful for your support and encouragement during my writing period.

Conflicts of interest: The authors declare that they have no known competing financial interests or personal relationships that could have appeared to influence the work reported in this paper.

Author's contribution: Jia Zelin and Meng Qinglei wrote the article, Wang Haifeng, Yu Ming, Zhang Xin, Cui Jiayu, Xiong Huisheng and Zhang Yuhang searched for information, and Wang Xueli corrected the article.

REFERENCES

- Baek B, Park YH, Jeon J-M, et al., 2025. Optimizing MALDI-TOF Mass Spectrometry for the Identification of Bacillus cereus: The Impact of Sporulation and Cultivation Time. Int J Mol Sci 26:4355.
- Calvigioni M, Cara A, Celandroni F, et al., 2022. Characterization of a Bacillus cereus strain associated with a large feed-related outbreak of severe infection in pigs. J Appl Microbiol 133:1078–1088.
- Chatelanat O, de Lorenzi-Tognon M, Spahr L, et al., 2024. Liver failure after *Bacillus cereus* food poisoning, an under-recognized entity: A case report. World J Hepatol 16:1339–1347.
- Chen H, Malengo G, Wang L, et al., 2025a. Coordination of virulence factors and lifestyle transition in Pseudomonas aeruginosa through single-cell analysis. Commun Biol 8:1236.
- Chen K, Li L, Wang N, et al., 2025b. Newly identified c-di-GMP pathway putative EAL domain gene STM0343 regulates stress resistance and virulence in Salmonella enterica serovar Typhimurium. Vet Res 56:13
- Chen Y, He Y, Meng Q, et al., 2023. Prokaryotic expression and biological activities of the hemolysin BL subunit of a pathogenic Bacillus cereus of cattle origin. Shengwu Gongcheng Xuebao/Chinese Journal of Biotechnology 39:4939–4949.
- Duport C, Jobin M and Schmitt P, 2016. Adaptation in Bacillus cereus: From Stress to Disease. Front Microbiol 7.

- Fagerlund A, Smith V, Røhr ÅK, et al., 2016. Cyclic diguanylate regulation of *Bacillus cereus* group biofilm formation. Mol Microbiol 101:471–494.
- Fang C, Hu W, Fang X, et al., 2025. Transcriptomic analysis reveals differential gene expression in spleen cells of Chinese soft-shelled turtle infected with Bacillus cereus BC12. Arch Microbiol 207:198.
- Fazli M, Almblad H, Rybtke ML, et al., 2014. Regulation of biofilm formation in <scp> P </scp> seudomonas and <scp> B </scp> urkholderia species. Environ Microbiol 16:1961–1981.
- Fei P, Yuan X, Zhao S, et al., 2019. Prevalence and Genetic Diversity of Bacillus cereus Isolated from Raw Milk and Cattle Farm Environments. Curr Microbiol 76:1355–1360.
- Fox D, Mathur A, Xue Y, et al., 2020. Bacillus cereus non-haemolytic enterotoxin activates the NLRP3 inflammasome. Nat Commun 11:760
- Gao X, Mukherjee S, Matthews PM, et al., 2013. Functional Characterization of Core Components of the Bacillus subtilis Cyclic-Di-GMP Signaling Pathway. J Bacteriol 195:4782–4792.
- Hermanas TM, Subramanian S, Dann CE, et al., 2021. Spore-Associated Proteins Involved in c-di-GMP Synthesis and Degradation of Bacillus anthracis. J Bacteriol 203.
- Heydenreich R, Nacita J, Lin C-W, et al., 2025. Revisiting bacterial spore germination in the presence of peptidoglycan fragments. J Bacteriol 207.
- Komprda T, Cwiková O, Kumbár V, et al., 2025. Key Factors Influencing Bacillus cereus Contamination in Hot Ready-to-Eat Meal Delivery. Foods 14:2605.
- Kunz S, Tribensky A, Steinchen W, et al., 2020. Cyclic di-GMP Signaling in Bacillus subtilis Is Governed by Direct Interactions of Diguanylate Cyclases and Cognate Receptors. MBio 11.
- Leguérinel I, Mathot A-G, Camarero A, et al., 2025. Modeling the effect of peracetic acid/hydrogen peroxide solution concentration and temperature treatment on *Bacillus cereus* spores inactivation. Lett Appl Microbiol 78.
- Li S, Bi C, Xiang B, et al., 2025. The role of cyclic di-GMP in biomaterialassociated infections caused by commensal Escherichia coli. PLoS One 20:e0330229.
- Mahler H, Pasi A, Kramer JM, et al., 1997. Fulminant Liver Failure in Association with the Emetic Toxin of Bacillus cereus. New England Journal of Medicine 336:1142–1148.
- Mao L, Li J, Huo X, et al., 2025. c-di-GMP regulates bacterial NAD biosynthesis via targeting the transcriptional repressor NadR. MBio
- Meng Q, Song L, Chi S, et al., 2025. Effect of environmental stress factors on the expression of virulence genes and pathogenicity of lethal Bacillus cereus of bovine origin. Front Microbiol 16.
- Mustafa A, Al Riyami B, Ow-Young-Villarreal G, et al., 2025. Structural and functional analysis of Bacillus cereus spore cortex lytic enzymes and YlaJ/YhcN lipoproteins. Microbiology (N Y) 171.
- Mustafa A-E-RA, Abo-Kamer AM and Al-Madboly LA, 2025. Bacillus cereus-derived α-amylase disrupts biofilm formation and quorum sensing in multidrug-resistant Klebsiella pneumoniae. BMC Microbiol 25:563.
- Ni B, Chang J, Zhou Y, et al., 2025. The coordinated regulatory impact of AcsS and TpdA on biofilm formation in Vibrio parahaemolyticus. Front Microbiol 16.
- Povolotsky TL and Hengge R, 2012. 'Life-style' control networks in Escherichia coli: Signaling by the second messenger c-di-GMP. J Biotechnol 160:10–16.
- Ramm F, Stech M, Zemella A, et al., 2021. The Pore-Forming Hemolysin BL Enterotoxin from Bacillus cereus: Subunit Interactions in Cell-Free Systems. Toxins (Basel) 13:807.
- Römling U, Galperin MY and Gomelsky M, 2013. Cyclic di-GMP: the First 25 Years of a Universal Bacterial Second Messenger. Microbiology and Molecular Biology Reviews 77:1–52.
- Saikia L, Medhi D, Bora S, et al., 2024. An Outbreak of Bacillus cereus Emetic Toxin Mediated Food Poisoning After Consumption of Fried Rice in Assam. Indian | Microbiol 64:957–962.
- Schreiber N, Hackl G, Reisinger AC, et al., 2021. Acute Liver Failure after Ingestion of Fried Rice Balls: A Case Series of Bacillus cereus Food Poisonings. Toxins (Basel) 14:12.
- Song LZLJWBZLYCYWX, 2019. Isolation, identification and virulence gene detection of a bovine-derived Bacillus cereus strain. Acta Agriculturae Boreali-Occidentalis Sinica 1735–1741.
- Subanna ARNS, Singh AK, Paschapur AU, et al., 2025. Genomic characterization and pathogenic mechanisms of Bacillus cereus WGPSB-2 isolated from the Himalayas. New Microbes New Infect 67:101616.

- Sun T, Wang R, Sun Y, et al., 2025. The Global Prevalence of Bacillus spp. in Milk and Dairy Products: A Systematic Review and Meta-Analysis. Foods 14:2599.
- Tawale RM, Ibrahim R and Aranjani JM, 2025. Updates on therapeutic targeting of diguanylate cyclase for addressing bacterial infections: A comprehensive review. World | Microbiol Biotechnol 41:317.
- A comprehensive review. World J Microbiol Biotechnol 41:317.

 Tong C, Xiao D, Li Q, et al., 2024. First insights into the prevalence, genetic characteristics, and pathogenicity of Bacillus cereus from generations worldwide. MSphere 9.
- Toyofuku M, Inaba T, Kiyokawa T, et al., 2016. Environmental factors that shape biofilm formation. Biosci Biotechnol Biochem 80:7–12.
- Wang X, 2023. Study on the Role of Second Messenger c-di-GMP in Bacillus cereus Strain 0-9.
- Whitfield GB, Marmont LS, Bundalovic-Torma C, et al., 2020. Discovery and characterization of a Gram-positive Pel polysaccharide biosynthetic gene cluster. PLoS Pathog 16:e1008281.
- Wu Z, Tian M, Fu S, et al., 2025. Spatial integration of sensory input and motor output in Pseudomonas aeruginosa chemotaxis through colocalized distribution. Elife 13.
- Xiao Z, Cheng M, Hu X, et al., 2023. Pathological changes of highly pathogenic Bacillus cereus on Pelodiscus sinensis. Veterinary Quarterly 43:1–10.
- Zhang P, Yao H, Ji L, et al., 2025. Epidemiological and genomic characterization of a rare foodborne outbreak caused by Bacillus paranthracis in Huzhou, China, 2024. Int J Food Microbiol 439:111265.